Quantitative performance of a polarization diffraction grating polarimeter encoded onto two liquid-crystal-on-silicon displays

Aarón Cofré[1,2,*], Asticio Vargas[2], Fabián A. Torres-Ruiz[2], Juan Campos[3], Angel Lizana[3], María del Mar Sánchez-López[4] and Ignacio Moreno[1]

1. Departamento de Ciencia de Materiales, Óptica y Tecnología Electrónica, Universidad Miguel Hernández de Elche, 03202 Elche, Spain
2. Departamento de Ciencias Físicas, Universidad de La Frontera, Temuco, Chile
3. Departamento de Física, Universidad Autónoma de Barcelona, Barcelona, Spain
4. Instituto de Bioingeniería. Departamento de Física y Arquitectura de Computadores, Universidad Miguel Hernández de Elche, 03202 Elche, Spain

* Corresponding Author: Aarón Cofré: acofre@umh.es

Abstract

We present a quantitative analysis of the performance of a complete snapshot polarimeter based on a polarization diffraction grating (PDGr). The PDGr is generated in a common path polarization interferometer with a Z optical architecture that uses two liquid-crystal on silicon (LCoS) displays to imprint two different phase-only diffraction gratings onto two orthogonal linear states of polarization. As a result, we obtain a programmable PDGr capable to act as a simultaneous polarization state generator (PSG), yielding diffraction orders with different states of polarization. The same system is also shown to operate as a polarization state analyzer (PSA), therefore useful for the realization of a snapshot polarimeter. We analyze its performance using quantitative metrics such as the conditional number, and verify its reliability for the detection of states of polarization.

KEYWORDS: Polarimeter, Polarization Diffraction Gratings, Spatial Light Modulators

1. INTRODUCTION

Polarimetry is a light-measuring technique [1] used in many different applications such as materials inspection [2], remote sensing [3], astronomy [4], biomedical applications [5], ophthalmology [6], among others. Due to this large amount of applications, there exist many different polarimeter systems proposed in the literature, each one presenting its particular characteristics. In general, we can distinguish between Stokes and Mueller polarimeters, if they are light-measuring or sample-measuring devices. Polarimeters can also be grouped as

punctual beam or image polarimeters, depending on their capability to differentiate polarization spatial variations. Finally, we can distinguish between time-sequential or snapshot polarimeters.

When dealing with real-time applications, the use of snapshot polarimeters is mandatory. There are a number of snapshot polarimeters described in the literature, which are mainly based on amplitude-division (AD) or wavefront-division (WD) architectures. AD polarimeters [7-10] are usually based on optical arrangements where the input beam is split in different sub-beams by using a collection of beam-splitters or prisms. Those sub-beams are then simultaneously analyzed by means of different polarization analyzers (PA) (i.e., different states of polarization where the input beam is projected). Those PAs are commonly achieved by placing different combinations of linear retarders and polarizers on the different sub-beams. A minimum number of 4 independent PAs are required. In general, the systems are bulky and require of synchronization between different radiometers to simultaneously record the different flux measurements. On the contrary, WD polarimeters [3,11] are usually based on a set of PAs that measure different parts of the input wavefront.

In this manuscript we design, optimize and implement a new type of AD polarimeter based on polarization diffraction gratings (PDGr), capable to perform punctual beam, snapshot and complete polarization metrology. PDGrs have been studied since many years, and they have been proposed for polarimetric measurements [12]. They are diffraction gratings based on a one-dimensional local periodic variation of the polarization transmission [13] and they are usually designed to be either polarizer or waveplate periodic structures, where the orientation of the transmission axis of the polarizer [14], or the principal axis of the wave-plate is periodically rotated [15].

Initial experimental realizations of PDGr based polarimeters were based on using micro-structured PDGr designed for IR light with large wavelengths [16]. The realization of PDGr for visible wavelengths required advances in microfabrication processes [17-19]. Recently, PDGr have been proposed for different types of polarimeters [20,21]. An alternative to produce PDGr has been the well stablished liquid-crystal technology. For instance, PDGr were demonstrated with ferroelectric displays [22,23], or with parallel-aligned nematic displays [24-26], and a punctual beam time-sequential polarimeter based on a simple PDGr was demonstrated in [27]. However, liquid crystal displays present limitations in the polarization states that can be generated, and this limits the types of PDGr that can be implemented. Therefore, these above mentioned PDGr can not be applied to produce a complete single-shot polarimeter.

Recently a new concept for generating PDGr was introduced in [28]. In this work, the PDGr was generated by encoding two independent phase-only diffraction gratings on two orthogonal states of polarization. The phase-only gratings were designed according to the optimal method for designing laser beam splitters [29]. This is a powerful grating design method, which can be used to select a number of target diffraction orders with a given constraint in their relative intensities [30] and/or phases [31]. The proper combination of two of such gratings, each one affecting different and orthogonal states of polarization, can be used to design arbitrary PDGrs, as demonstrated in Ref. [28]. In that work, an optical reflective architecture was used, employing a special transmissive parallel-aligned liquid crystal display. However, reflective liquid-crystal on silicon (LCoS) displays are much more common and commercially available nowadays.

In this work, we show an alternative optical architecture based on two LCoS displays to encode PDGr following the technique initiated in [28]. In addition, we analyze the implementation of a snapshot punctual polarimeter based on this system. The proposed polarimeter system is capable of simultaneously generate all the required PAs. Moreover, alignment of the set-up is not extremely demanding as occurring in other polarimeter proposals. In addition, as the LCoS performance can be optimized to different wavelengths, simply by addressing the proper electrical sequences [32], the proposed set-up could be used to perform multi-channel polarimetry.

The outline of this manuscript is as follows. In section 2, we first introduce the optical architecture and describe the details of the experimental system. Then, in section 3, we present the design of the two optimal phase-only gratings that constitute the PDGr. Section 4 presents the experimental results. The accuracy and quality of the PDGr based polarimeter are quantified according to well stablished quality metrics. Finally, Section 5 presents the conclusions of the work.

2. OPTICAL ARCHITECTURE

Figure 1 shows the scheme of the optical setup. The polarimeter comprises two LCoS spatial light modulators in a Z configuration. An input He-Ne laser (λ=633 nm) is first spatially filtered and collimated by means of lens L1. A polarization state generator (PSG) composed of a linear polarizer (P1) and a quarter wave-plate (QWP) is used to control the state of polarization of this beam before it reaches the first modulator. This PSG is used in the calibration step and in the performance analysis to introduce in the polarimeter beams with known polarization states.

The two modulators are arranged in a Z configuration as indicated in Fig. 1. The angle between the incident ray and the reflected ray on each modulator is of β=11°. Modulators LCoS1 and LCoS2 are conjugated planes by means a 4f system obtained with two lenses L2 and L3, with the same focal length, f=200 mm, thus obtaining a unit magnification. Both modulators are parallel-aligned LCOS displays, with the liquid crystal director aligned horizontally with respect to the laboratory framework. They are modulators from Holoeye, Pluto model, with 1920x1080 pixels and 8 μm pixel pitch. LCoS1 is designed to operate in the visible range, while LCoS2 is originally designed to operate in the near infrared range (NIR II). This kind of devices have been extensively used for displaying phase-only diffraction gratings [33]. The retardance versus addressed gray level was previously calibrated for both modulators for the wavelength of 633 nm, following the method described in Ref. [34]. The results are shown in Fig. 2. LCoS1 display provides a phase modulation depth up to more than 2π in the complete gray level range, while LCoS2 display reaches the 2π phase modulation for a gray level less than 100.

Parallel-aligned LCoS displays only modulate the linear polarization component parallel to the LC director. In our devices, this corresponds to the horizontal direction. Therefore, a phase pattern addressed to LCoS1 modulates the horizontal component of the input beam. A half-wave plate (HWP) is added after lens L3, oriented at 45°, to transform the horizontal linear polarization component into the vertical polarization component and vice versa. Then, the beam illuminates the LCoS2 display. A phase pattern addressed to this second display is therefore now encoded on the original vertical polarization component in the input beam

(which was unaffected by LCoS1). In this way, the two orthogonal horizontal and vertical polarization components of the input beam can be independently modulated with these two modulators.

Finally, the Fourier transform plane is retrieved at the back focal plane of another convergent lens L4, with focal length f=150 mm, and a microscope objective (10X) produces a magnified image onto a CCD Basler piA1000 60gm camera. When necessary, an analyzer (P3) is placed in between the objective and the camera to select the appropriate polarization component.

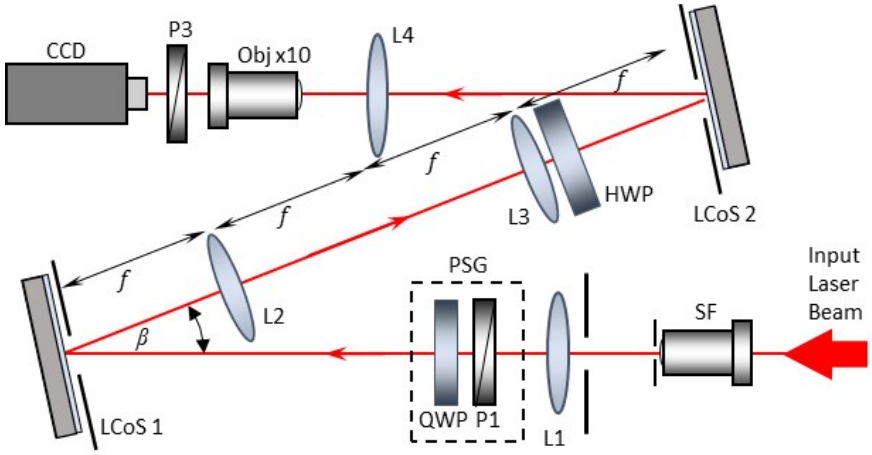

Figure 1. Scheme of the optical setup. LCoS1 and LCoS2 are two liquid-crystal on silicon displays, with the liquid crystal director oriented horizontally. SF is a spatial filter. PSG is an input polarization state generator composed of a linear polarizer and a quarter-wave plate. A 4f-system images LCoS1 onto LCoS2. A CCD captures the magnified images by an objective (10X). An analyzer (P3) selects the information to be captured in the CCD detector. The angle β is 11°.

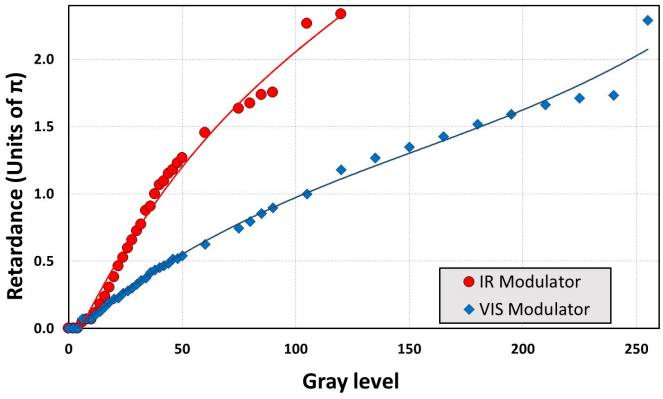

Figure 2. Phase modulation of the LCoS1 (VIS modulator) and LCoS2 (IR modulator) versus addressed gray level. Dots indicate experimental measurements and lines indicate the fitting curves.

3. POLARIZATION GRATING DESIGN

The PDGr design used in this experiment has been previously described in Ref. [28]. It is designed to work as a PSG that yields six target diffraction orders k=±1, ±2, ±3, when it is illuminated with linearly polarized light oriented at 45º, where the states of polarization in each order correspond to linear states oriented at 0°, 45°, 90° and 135°, and the two circular right (RCP) and left (LCP) states.

The above-stated polarizations are generated by addressing a different phase-only diffraction grating to the LCoS1 and LCoS2 displays, one modulating the initial horizontal polarization component (Grating H) and the other modulating the initial vertical polarization component (Grating V). Following [28], these phase-only gratings are calculated as:

$$\exp\left(i\phi(x)\right) = \frac{g(x)}{|g(x)|} = \sum_{k=-\infty}^{+\infty} G_k \exp\left(i2\pi kx / D\right), \tag{1}$$

where

$$g(x) = \sum_{k\in T} \mu_k e^{i\alpha_k} \exp(i2\pi kx / D). \tag{2}$$

Here in Eq. (2) the summation is performed only on the selected set (T) of target diffraction orders. D denotes the period of the grating. μ_k and α_k are numerical parameters that must be determined numerically to fulfill the required restrictions on the Fourier coefficients G_k of the phase only gratings in Eq. (1). These Fourier coefficients are complex numbers

$$G_k = |G_k| \exp\left(i\beta_k\right). \tag{3}$$

Therefore, restrictions can be imposed on the intensity $i_k = |G_k|^2$ of the target diffraction orders, on their phases β_k, or in both magnitudes. The efficiency of the grating design (η) is defined as the summation of the relative intensities in the target orders, i.e. [28]:

$$\eta = \sum_{k\in T} i_k = \sum_{k\in T} |G_k|^2 . \tag{4}$$

Table 1 provides the numerical data that yields the specific PDGr design used in this work. It is composed of two phase-only gratings, each one producing five diffraction orders. Table 1 provides also the information about the restrictions in the relative intensities and the phases β_k imposed on each phase-only grating, as well as the corresponding numerical solution given by parameters μ_k and α_k.

Orders k=+2, and k=-2 are present only in the V and H gratings, respectively (see Table 1). This way, these diffraction orders encode, respectively, linear polarizers in the vertical and in the horizontal direction. On the contrary, orders k=±1, and k=±3 are present in both gratings and have the same intensity, equal to half the intensity of the orders k=±2. Orders k=+2, and k=-2 are selected in the corresponding grating design with twice the relative intensity as the other target orders, to produce a PDGr where all six diffraction orders have the same weight.

Because orders k=±1, and k=±3 have equal contribution of both polarization components, they encode linear retarders, where the retardance in each diffraction order is given by the phase difference of the corresponding phases imposed on each grating, i.e.,

$$\Delta_k = \beta_k^V - \beta_k^H . \tag{5}$$

The phases β_k are imposed to provide retardances $\Delta_{+3} = -\pi/2$, $\Delta_{+1} = -\pi$, $\Delta_{-1} = +\pi/2$ and $\Delta_{-3} = 0$. This way, orders k=+3 and k=-1 encode quarter-wave retarders, with different sign in the retardance, while order k=+1 encodes a half-wave retarder. Note that the orientation of the neutral axes of these equivalent retarders is the vertical and the horizontal directions. Finally, order k=-3 encodes a full-wave retarder, thus not changing the input state of polarization.

The efficiency of the two phase diffraction gratings composing the PDGr is the same, η=87%, thus meaning that there is approximately 13% of the energy contributing to other non-target diffraction orders.

TABLE 1

Constrains imposed onto the H and V gratings to generate the desired PDGr, and the corresponding numerical solution. The efficiency in both gratings is η = 87%.

	Grating H				Grating V				
Order	**Rel.Int**	β_k	μ_k	α_k	**Rel.Int**	β_k	μ_k	α_k	Δ
+3	½	-3π/4	1.2691	5.3103	½	3π/4	0.8163	4.1848	π/2
+2	-	-	-	-	1	-	1.1748	0.2646	-
+1	½	π/2	1.2294	2.9620	½	-π/2	0.9751	0.2364	-π
-1	½	-π/4	0.7487	0.6004	½	π/4	0.8385	2.6531	-π/2
-2	1	-	1.4377	-0.5776	-	-	-	-	-
-3	½	0	0.8603	1.4055	½	0	0.7366	1.6691	0

Figure 3 shows the phase profile for the H and V phase–only gratings respectively, as a function of the spatial coordinate x along one period D of the gratings. Modulators LCoS1 and LCoS2 respectively must encode these non-linear continuous profiles. The correct reproduction of these phase profiles in pixelated displays requires large periods in the grating, since enough pixels per period are necessary to reproduce these profiles with enough accuracy. The use of high-resolution displays as the LCoS devices used in this work represents an improvement with respect to the previous system in Ref. [28]. The grating period in this work is selected to be of 50 pixels, thus the PDGr has a period of 400 μm.

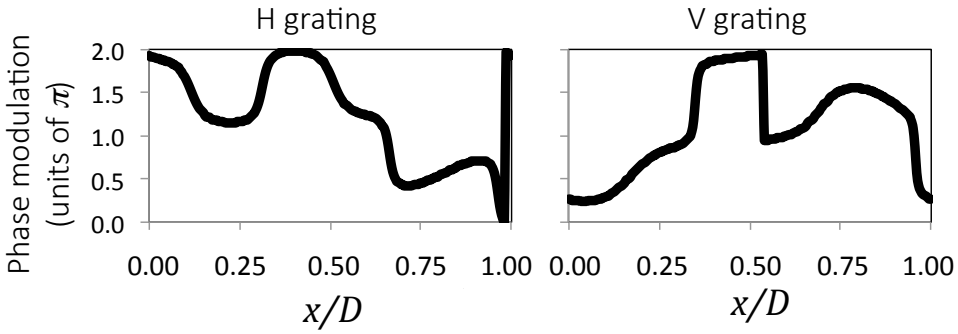

Figure 3. Phase profiles in one period of the gratings displayed in modulators LCoS1 (H grating) and LCoS2 (V grating) to compose the PDGr.

4. CALIBRATION OF THE PDGr POLARIMETER

The polarization design described in section 3 shows how to generate a particular polarization basis by means of a PDGr. In this section, the idea is to use the system in reverse sense. Hence we are setting a basis of polarization analyzers (PAs) that defines our polarization state detector. To this aim, note that the final linear analyzer (P3 in the system in Fig. 1), oriented at 45°, is required in the system. In particular, since the PDGr generates six diffraction orders, each one reproducing a given polarization element (two linear polarizers oriented horizontally and vertically, and four retarders), we therefore have six different polarization state analyzers (PAs) acting simultaneously.

To test the PDGr polarimeter, we select different states of polarization in the input beam by properly adjusting the PSG elements in Fig. 1. We choose to calibrate the polarimeter

with the six cardinal states: input linear states oriented at 0°, 45°, 90° and 135°, and the two circular states RCP and LCP. Figure 4 presents the corresponding images captured at the CCD camera for each of these input polarizations. The PAs expected in each diffraction order are indicated on the bottom of the image. Note that the PDGr generates six fixed diffraction orders, but the intensity in each order depends on the specific input state of polarization. Therefore, these arrays of intensities detected at the CCD camera can be understood as the simultaneous projection of the input polarization on the six PAs basis set by the PDGr.

For instance, when the input polarization is linear and vertical, Fig. 4(a), the diffraction order k=-2 vanishes, while the diffraction order k=+2 is the strongest one. This is in agreement with the expected realization of horizontal and vertical linear polarizer analyzers at these orders respectively. The other four orders, k=-3, -1, +1 and +3, show approximately the same intensity, half of the intensity in order k=+2. Again, this is in accordance with the expected actuation of different linear retarders in these four orders. Note that, since the vertical direction coincides with a neutral axis in the retarders encoded in these four orders, the input polarization is not modified, and it is projected with half intensity to the final analyzer P3 oriented at 45°.

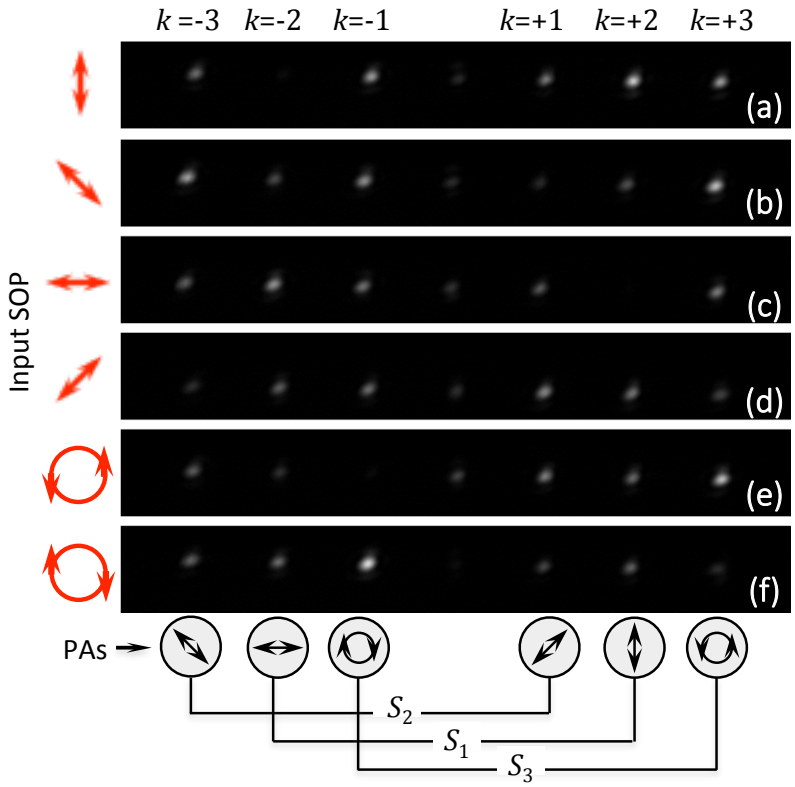

Figure 4. CCD captures for the calibration of the PDGr polarimeter with six different input states of polarization (SOP) indicated in the left. The polarization analyzers (PAs) for each diffraction order are drawn on the bottom.

For the other input states of polarization shown in Fig. 4, the intensities at the six diffraction orders follow the expected behavior. In each case, there is one bright diffraction order that corresponds to the positive detection of the input polarization, four diffraction orders with equal intensity, and a diffraction order that is cancelled, corresponding to the polarization orthogonal to the input one. The six PAs allow, in principle, a snapshot and complete measurement of the input Stokes parameters by simply subtracting the intensities in

the pair of diffracted orders corresponding to orthogonal analyzers, as indicated in the bottom of the figure.

However, although the results in Fig. 4 show qualitatively the expected behavior, the actual quantitative values might show discrepancies. There are several factors that affect these results: the accuracy in the reproduction of the phase-only gratings composing the PDGr, the phase modulation quality of the employed LCoS displays (which are affected by phase fluctuations [35]), the number of pixels used to encode the continuous phase-only gratings, the quality of the optical elements in the system, etc. Therefore, in order to consider all these effects for a practical application of such PDGr polarimeter, a quantitative precise calibration must be performed.

There exists different means to calibrate the analysis matrix $\mathbf{A}$, the matrix whose rows represent the different polarization analyzers of a Stokes polarimeter. The calibration procedure used here is given next in detail, and follows an inversion procedure, as those described in Refs. [1,36]. First, we define the $\mathbf{S}$ matrix, whose rows define the Stokes vectors corresponding to the six selected input states of polarization used in Fig. 4, i.e.:

$$\mathbf{S} = \begin{pmatrix} 1 & 1 & 1 & 1 & 1 & 1 \\ 0 & 0 & 1 & 0 & -1 & 0 \\ 0 & 0 & 0 & 1 & 0 & -1 \\ 1 & -1 & 0 & 0 & 0 & 0 \end{pmatrix}. \tag{6}$$

Then, for each of these input states, the intensity at the six diffraction orders is measured. These values are retrieved from the images shown in Fig. 4. This leads to the flux-matrix $\mathbf{I}$, which is a 6×6 matrix that contains the measured intensities at each of the 6 diffraction orders, for each of the six input states of polarization (SOPs) used in the calibration. Matrices $\mathbf{I}$ and $\mathbf{S}$ are related by the following linear system:

$$\mathbf{I} = \mathbf{A} \cdot \mathbf{S}, \tag{7}$$

where $\mathbf{A}$ is the analysis matrix, in this case a 6×4 matrix that defines the action of the six PAs elements in our experimental PDGr polarimeter system. The analysis matrix can be explicitly determined as [36]:

$$\mathbf{A} = \mathbf{I} \cdot \mathbf{S}^t \cdot \left(\mathbf{S} \cdot \mathbf{S}^t \right)^{-1}, \tag{8}$$

where *t* indicates the transposed matrix, and $\mathbf{S}^t \cdot \left(\mathbf{S} \cdot \mathbf{S}^t \right)^{-1}$ is the pseudo-inverse of the $\mathbf{S}$ matrix.

Thus, the matrix $\mathbf{A}$ was determined numerically according to Eq. (8), from the experimental data in Fig.4 (i.e., matrix $\mathbf{I}$), and the result we obtained is:

$$\mathbf{A} = \begin{pmatrix} 1.43 & 0.10 & 0.83 & 0.05 \\ 1.13 & -0.97 & -0.15 & 0.40 \\ 1.76 & 0.30 & 0.23 & 1.52 \\ 1.32 & 0.19 & -0.67 & -0.42 \\ 1.37 & 1.33 & -0.24 & -0.08 \\ 1.77 & 0.17 & 0.85 & -0.99 \end{pmatrix}. \tag{9}$$

Once the analysis matrix $\mathbf{A}$ is calibrated, an unknown input polarization (described by its Stokes vector $\mathbf{S}$) can be determined by experimentally measuring the intensity matrix $\mathbf{I}$ in Eq. (7) and by mathematically inverting the matrix $\mathbf{A}$. However, performing the inverse of the matrix $\mathbf{A}$, introduces a certain amount of experimental noise that can be amplified from the

intensity matrix $\mathbf{I}$ to the final measurement of the Stokes parameters $\mathbf{S}$. To estimate the quality of the analysis matrix $\mathbf{A}$ in terms of noise amplification, different well-known metrics, as the conditional number (CN) or the equally weighted variance (EWV) indicator can be used [37]. In this work, we use the conditional number, which is defined as [38]

$$CN(\mathbf{A}) = \frac{\sigma_{\max}}{\sigma_{\min}}. \tag{10}$$

where $\sigma_{\max}$ and $\sigma_{\min}$ are, respectively, the maximum and minimum singular values different from zero of matrix $\mathbf{A}$. Minimizing this parameter leads to the optimal system in terms of polarimeter measurements.

The CN for the ideal analysis $\mathbf{A}$ matrix calculated from the theoretical PAs basis set by our PDGr polarimeter is CN=1.73, i.e., the best possible value achievable for polarimetric systems [3,37]. In the case of the experimentally measured $\mathbf{A}$ matrix (Eq. (9)), the corresponding conditional number is CN=2.97 which is close to the best situation (CN=1.73) and comparable with our previous system using sequential measurements [27].

The experimental conditional number of the implemented system ensures a good polarimeter performance in terms of noise amplification. However, if an even better conditioning is required, the system may be further optimized. In fact, as stated above, one of the main discrepancies between the theoretical-experimental CN values is related to the time-fluctuations phenomenon occurring in some LCoS displays and discussed in Ref. [35]. These fluctuations modify the LCoS performance changing the addressed PDGr as a function of the time, especially in the case of the IR-based LCoS display (we are using a wavelength outside the recommended wavelength range). This situation could be improved by using two LCoS optimized for the operating wavelength, and by applying some of the available methods devised to decrease the effect of the phase fluctuations [39,40]. However, as we show next, the obtained experimental CN is suitable enough to ensure polarimetric measurements with small values of noise amplification, and therefore, to prove the suitability of the PDGr polarimeter to perform polarimetric metrology.

5. RESULTS AS A SNAPSHOT POLARIMETER

In this section, we present the application of the previously calibrated PDGr polarimeter to take snapshot punctual Stokes polarimetric measurements. For that purpose, we illuminate the system with an unknown state of polarization (labeled with the subscript m), and measure the intensities detected at each of the six target diffraction orders. The result is a $\mathbf{I}_m$ (6x1) matrix, which is related to the Stokes parameters ($\mathbf{S}_m$, 4x1 matrix) by the calibrated $\mathbf{A}$ matrix,

$$\mathbf{I}_m = \mathbf{A} \cdot \mathbf{S}_m, \tag{11}$$

This matrix relation can be inverted to directly provide the Stokes parameters of the input beam as

$$\mathbf{S}_m = \left(\mathbf{A}^t \cdot \mathbf{A}\right)^{-1} \mathbf{A}^t \cdot \mathbf{I}_m = \tilde{\mathbf{A}}^{-1} \cdot \mathbf{I}_m, \tag{12}$$

where the matrix $\tilde{\mathbf{A}}^{-1} = \left(\mathbf{A}^t \cdot \mathbf{A}\right)^{-1} \mathbf{A}^t$ is the pseudo-inverse matrix of the $\mathbf{A}$ matrix. The Stokes parameters $\mathbf{S}_m$ is the experimental polarimetric measurement. The azimuth angle (α) and ellipticity angle (ε) are calculated from them as [41]:

$$\tan(2\alpha) = \frac{S_2}{S_1}, \tag{13}$$

$$\sin(2\varepsilon) = S_3, \tag{14}$$

and the angle and phase between the electric field components are calculated as

$$\tan(2\chi) = \frac{\sqrt{S_2^2 + S_3^2}}{S_1}, \tag{15}$$

$$\tan(\delta) = \frac{S_3}{S_2}, \tag{16}$$

To test the polarimeter performance, we first selected the input PSG to reproduce three of the states of polarization selected for the polarimeter calibration: horizontal linear polarization, linear polarization oriented at 45°, and left circular polarization. The corresponding results are presented in Fig. 5. The figure shows the polarization ellipse as well as the representation in the Poincaré sphere. In addition, each analyzed case shows the theoretical expected result, in blue, superimposed with the experimentally measured polarization state, in red. The agreement is almost perfect, as it should be expected since these states were used for the calibration of the system.

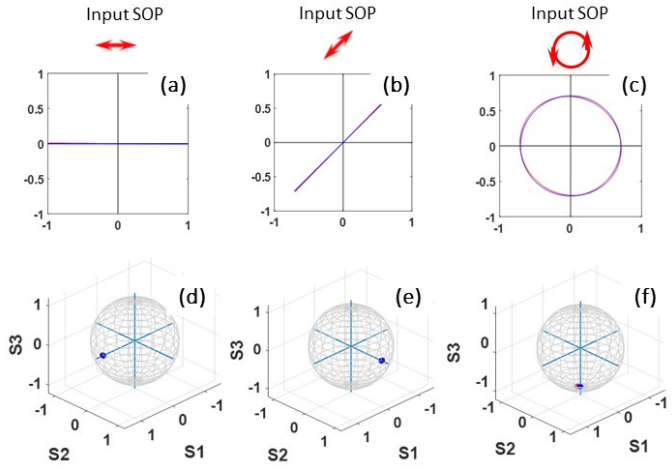

Figure 5. Performance of the polarimeter for SOPs used in the calibration process: Linear 0°, 45° and left circular polarizations. Blue points and lines are theoretical results. Red points and lines are the experimental results obtained from polarimeter information.

Next, we further explored the polarimeter performance by measuring input SOPs different from those used in the calibration. Two different arbitrary input SOPs were selected by modifying the orientation of the optical elements in our PSG system. Table 2 gives the values for these two configurations. In the first one (SOP1), the input polarizer P1, and the input quarter-wave plate QWP in the PSG (see Fig. 1) are both oriented with an angle of 120°, thus SOP1 is a linear state with an azimuth of 120°. In the second configuration (SOP2), we selected P1 with an angle zero, while the QWP is oriented at 30°. The resulting input state is therefore an elliptical state with an azimuth and ellipticity angles both of 30°.

Figure 6 shows the experimental polarimetric measurements obtained. Figures 6(a) and 6(d) show the image captured at the CCD camera for these two input SOPs respectively. In both cases, the six target diffraction orders are clearly visible, although their relative intensities are different in each case. From these recorded intensities, the SOP is calculated numerically

using Eqs. (12)-(14). Figures 6(b) and 6(c) show the polarization ellipse and its representation in the Poincaré sphere for SOP1. Again, in blue we indicate the expected state, and in red the measured one. Figures 6(e) and 6(f) show the equivalent results for SOP2. Finally, Table 2 gives the retrieved experimental values, which show a very good agreement with the theoretical values. Thus, all these results validate the performance of the proposed new grating polarimeter.

TABLE 2

Theoretical and experimental states of polarization of the two PSG configurations selected to verify the performance of the PDGr snapshot polarimeter.

SOP1 (P1: 120°; QWP: 120°)			**SOP2 (P1: 0°; QWP: 30°)**		
	Theory	Experiment		Theory	Experiment
Azimuth (α)	-60.0°	-60.6°	Azimuth (α)	30.0°	31.5°
Ellipticity (ε)	0.0°	-1.4°	Ellipticity (ε)	30.0°	29.0°
Angle (χ)	60.0°	60.5°	Angle (χ)	37.7°	38.1°
Phase (δ)	180.0°	-176.7°	Phase (δ)	63.4°	60.8°

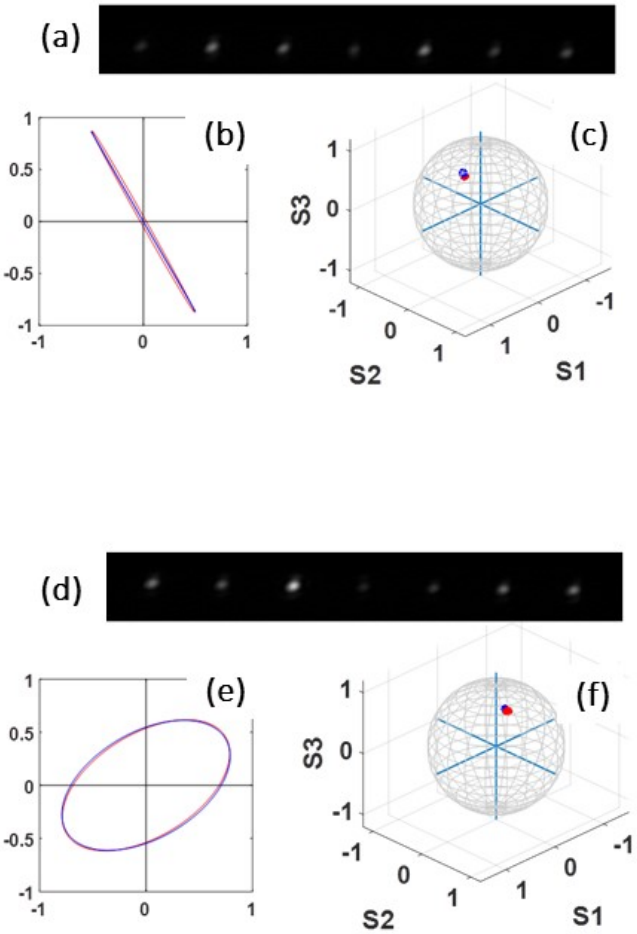

Figure 6. Experimental results to validate the PDGr polarimeter performance using input SOPs different to those employed in the calibration. SOP1: linear polarization with azimuth of 120°. (a) Experimental diffraction orders, (b) polarization ellipse, and (c) Poincaré sphere representation. SOP2: elliptical polarization with azimuth of 30° and ellipticity of 30°. (d) Experimental diffraction orders, (e) polarization ellipse, and (f) Poincaré sphere representation. Points and lines in blue and red indicate theoretical and experimental values respectively.

6. CONCLUSIONS

In summary, we have experimentally presented and validated a new type of snapshot punctual polarimeter based on the generation of a PDGr. Since the polarization measurements are obtained almost instantaneously (only limited by the refresh rate of the CCD camera), the proposed prototype may find interest in real-time applications. We have applied a PDGr design previously reported in [28], but we have used a different optical architecture with a Z configuration, that uses two commercial LCoS spatial light modulators (unlike Ref. [28], where a non-commercial transmissive parallel-aligned display was employed). The two displays are used to independently encode two phase-only diffraction gratings on two orthogonal states of polarization. The gratings are specifically designed to yield a combined polarization diffraction grating that generates six diffraction orders. Each of these diffraction orders encode a different polarization state analyzer, that correspond to the six states typically employed in polarimetric measurements: linear states at 0°, 45°, 90° and 135°, and the two circular states.

The use of LCoS displays is interesting since they provide a better spatial resolution, with larger number of pixels and smaller size. Therefore, they can implement the PDGr with more pixels per period and consequently better efficiency and quality of the PDGr is achieved.

We performed a quantitative calibration of the polarimeter system to calculate its performance. An experimental value of the conditional number CN=2.97 was obtained. The polarimeter has been validated experimentally, providing errors in the azimuth and ellipticity angles less than 2°. This level of accuracy makes the proposed PDGr-based polarimeter interesting, especially because of the great flexibility provided by the use of programmable LCoS displays. For instance, it can be very easily adapted to different wavelengths simply by changing the gray levels used in the grating.

Acknowledgements

This work has been financed by Ministerio de Economía, Industria y Competitividad of Spain and European Union (FEDER funds) through grants FIS2015-66328-C3-3-R (MINECO/FEDER, UE) and FIS2015-66328-C3-1-R (MINECO/FEDER, UE). A. Vargas and F. Torres-Ruiz acknowledge support from Fondecyt through grant 1151290. A. Cofré acknowledges Generalitat Valenciana for a grant of the Santiago Grisolia Program, ref. 2015/073.

[MINECO/FEDER, UE], financiado por el Ministerio de Economía, Industria y Competitividad y por la Unión Europea a través del Fondo Europeo de Desarrollo Regional - FEDER – "Una manera de hacer Europa"

References

1. R. A. Chipman, "Polarimetry," in *Handbook of Optics*, M. Bass, Edt. (McGraw-Hill, 1995).
2. A. Lizana, M. Foldyna, M. Stchakovsky, B. Georges, N. David, and E. Garcia-Caurel, "Enhanced sensitivity to dielectric function and thickness of absorbing thin film by combining total internal reflection ellipsometry with standard ellipsometry and reflectometry," J. Phys. D Appl. Phys. **46** (10), 105501 (2013).

3. J. Scott Tyo, D. L. Goldstein, D. B. Chenault, and J. A. Shaw, “Review of passive imaging polarimetry for remote sensing applications,” Appl. Opt. **45** (22), 5453-5469 (2006).

4. N. Uribe-Patarroyo, A. Alvarez-Herrero, R. L. Heredero, J. C. del Toro, A. C. López, V. Domingo, J. L. Gasent, L. Jochum, and V. Martínez, “IMaX: a polarimeter based on liquid crystal variable retarders for an aerospace mission,” Phys. Status Solidi C **5** (5), 1041–1045 (2008).

5. M. R. Antonelli, A. Pierangelo, T. Novikova, P. Validire, A. Benali, B. Gayet, and A. De Martino, “Mueller matrix imaging of human colon tissue for cancer diagnostics: how Monte Carlo modeling can help in the interpretation of experimental data,” Opt. Express **18** (10), 10200–10208 (2010).

6. J. M. Bueno, “Polarimetry using liquid-crystal variable retarders: Theory and calibration,” J. Opt. A **2**, 216–222 (2000).

7. E. Compain and B. Drevillon, “Broadband division-of-amplitude polarimeter based on uncoated prisms,” Appl. Opt. **37** (25), 5938-5944 (1998).

8. M. El-Saba, R. M. A. Azzam, and M. A. G. Abushagur, “Parallel-slab division-of-amplitude photopolarimeter,” Opt. Lett. **21** (21), 1709-1711 (1996).

9 R.M.A. Azzam, “Stokes-vector and Mueller-matrix polarimetry,” J. Opt. Soc. Am. A **33** (7), 1396-1408 (2016).

10. A. Peinado, A. Lizana, A. Turpin, C. Iemmi, T. K. Kalkandjiev, J. Mompart, and J. Campos, “Optimization, tolerance analysis and implementation of a Stokes polarimeter based on the conical refraction phenomenon,” Opt. Express **23**, 5636–5652 (2015).

11. O. Acher, S. Richard, and T.-L. Nguyen “Wavefront-division polarimetric analysis method and device, spectropolarimeter, polarimetric camera and optical microscope using such a device,” US patent US20150204724 A1 (2015).

12. T. Todorov and L. Nikolova, “Spectrophotopolarimeter: fast simultaneous real-time measurement of light parameters,” Opt. Lett. **17** (5), 358-360 (1992).

13. G. Cincotti, “Polarization gratings: Design and applications,” IEEE J. Quant. Electron. **39** (12), 1645-1652 (2003).

14. F. Gori, “Measuring Stokes parameters by means of a polarization grating,” Opt. Lett. **24** (9), 584-586 (1999).

15. J. Tervo and J. Turunen, “Paraxial-domain diffractive elements with 100% efficiency based on polarization gratings,” Opt. Lett. **25** (11), 785-786 (2000).

16. Z. Bomzom, G. Biener, V. Kleiner, and E. Hasman, “Spatial Fourier-transform polarimetry using space-variant subwavelength metal-stripe polarizers,” Opt. Lett. **26** (21), 1711-1713 (2001).

17. C. Oh and M. J. Escuti, “Achromatic diffraction from polarization gratings with high efficiency,” Opt. Lett. **33** (20), 2287-2289 (2008).

18. I. Vartiainen, J. Tervo, J. Turunen, and M. Kuittinen, “Surface-relief polarization gratings for visible light,” Opt. Express **18** (22), 22850-22858 (2010).

19. M. Beresna and P G. Kazansky, “Polarization diffraction grating produced by femtosecond laser nanostructuring in glass,” Opt. Lett. **35** (10), 1662-1664 (2010).

20. M. W. Kudenov, M. J. Escuti, E. L. Dereniak, and K. Oka, “White-light channeled imaging polarimeter using broadband polarization gratings,” Appl. Opt. **50** (15), 2283-2293 (2011).

21. M. W. Kudenov, M. J. Escuti, N. Hagen, E. L. Dereniak, and K. Oka, “Snapshot imaging Mueller matrix polarimeter using polarization gratings,” Opt. Lett. **37** (8), 1367-1369 (2012).

22. M. Le Docen and P. Pellat-Finet, “Polarization properties and diffraction efficiencies of binary anisotropic gratings: general study and experiments on ferroelectric liquid crystals,” Opt. Commun. **151** (4-6), 321-330 (1998).

23. A. Martínez-García, I. Moreno, M. M. Sánchez-López, P. García-Martínez, “Operational modes of a ferroelectric LCOS modulator for displaying binary polarization, amplitude and phase diffraction gratings,” Appl. Opt. **48** (15), 2903-2914 (2009).

24. J. A. Davis, J. Adachi, C. R. Fernández-Pousa, and I. Moreno, “Polarization beamsplitters using programmable polarization diffraction gratings,” Opt. Lett. **26** (9), 587-589 (2001).

25. C. R. Fernández-Pousa, I. Moreno, J. A. Davis, and J. Adachi, “Polarizing diffraction grating triplicators,” Opt. Lett. **26**, 1651-1653 (2001).

26. J. A. Davis, G. H. Evans, “Polarizing binary diffraction grating beam splitter”, Opt. Lett. **29** (13), 1443-1445 (2004).

27. A. Vargas, F. A. Torres-Ruiz, J. Campos, R. Donoso, J. L. Martínez, I. Moreno, “Flexible polarimeter architecture based on a birefringent grating,” Appl. Opt. **53** (25), 5585-5592 (2014)

28. J.A. Davis, I. Moreno, M. M. Sánchez-López, K. Badham, J. Albero, and D. M. Cottrell “Diffraction gratings generating orders with selective states of polarization,” Opt. Express **24** (2), 907-917 (2016).

29. L. A. Romero and F.M. Dickey, “The mathematical theory of laser beam-splitting gratings,” Prog. Optics **54**, 319–386 (2010).

30. J. Albero, I. Moreno, J. A. Davis, D.M. Cottrell, D. Sand, “Generalized phase diffraction gratings with tailored intensity,” Opt. Lett. **37** (20), 4227-4229 (2012).

31. J. Albero, J. A. Davis, D. M. Cottrell, C. E. Granger, K. R. McCormick, and I. Moreno, “Generalized diffractive optical elements with asymmetric harmonic response and phase control,” Appl. Opt. **52** (15), 3637-3644 (2013).

32. A. Hermerschmidt, S. Osten, S. Krüger and Thomas Blümel, "Wave front generation using a phase-only modulating liquid-crystal based micro-display with HDTV resolution,” Proc. SPIE **6584**, 65840E (2007).

33. Y. Lin, Y. Ai, X. Shan, M. Liu, “Liquid crystal based non-mechanical beam tracking technology,” Opt. Laser Technol. **91**, 103–107 (2017).

34. A. Vargas, R. Donoso, M. Ramírez, J. Carrión, M. M. Sánchez-López, I.Moreno, “Liquid crystal retarder spectral retardance characterization based on a Cauchy dispersion relation and a voltage transfer function,” Opt. Rev. **20** (5), 378–384 (2013).

35. A. Lizana, I. Moreno, A. Márquez, C. Iemmi, E. Fernandez, J. Campos and M. J. Yzuel, “Time fluctuations of the phase modulation in a liquid crystal on silicon display: characterization and effects in diffractive optics,” Opt. Express **16** (21), 16711-16722, (2008).

36. E. Garcia-Caurel, R. Ossikovski, M. Foldyna, A. Pierangelo, B. Drévillon and A. De Martino, “Advanced Mueller Ellipsometry Instrumentation and Data Analysis,” in *Ellipsometry at Nanoscale*, M. Losurdo and K. Hingerls (Edts.), pp. 31-143, Springer-Varlag, Berlin (2013).

37. A. Peinado, A. Lizana, J. Vidal, C. Iemmi and J. Campos, "Optimization and performance criteria of a Stokes polarimeter based on two variable retarders," Opt. Express **18**, 9815–9830 (2010).

38. P. Taylor, *Theory and Applications of Numerical Analysis*, (Academic Press, London, 1974).

39. A. Lizana, A. Márquez, L. Lobato, Y. Rodange, I. Moreno, C. Iemmi and J. Campos, "The minimum Euclidean distance principle applied to improve the modulation diffraction efficiency in digitally controlled spatial light modulators", Opt. Express **18** (10), 10581-10593, (2010).

40. J. García-Márquez, V. López, A. González-Vega, and E. Noé, "Flicker minimization in an LCoS spatial light modulator," Opt. Express **20** (8), 8431-8441 (2012).

41. D. Goldstein, *Polarized Light*, 2nd Edt. (Marcel Dekker, 2003).